# Raman-active Fröhlich optical phonon mode in arsenic implanted ZnO

J. D. Ye, S. Tripathy, Fang-Fang Ren, X. W. Sun, G. Q. Lo, and K. L. Teo

Citation: Applied Physics Letters **94**, 011913 (2009); doi: 10.1063/1.3067997
View online: http://dx.doi.org/10.1063/1.3067997
View Table of Contents: http://scitation.aip.org/content/aip/journal/apl/94/1?ver=pdfcov
Published by the AIP Publishing

# Raman-active Fröhlich optical phonon mode in arsenic implanted ZnO

J. D. Ye,[1,a)] S. Tripathy,[2] Fang-Fang Ren,[1] X. W. Sun,[1] G. Q. Lo,[1] and K. L. Teo[3]
[1]*Institute of Microelectronics, A*STAR (Agency for Science, Technology and Research), 11 Science Park Road, Singapore Science Park II, Singapore 117685, Singapore*
[2]*Institute of Materials Research and Engineering, A*STAR (Agency for Science, Technology and Research), 3 Research Link, Singapore 117602, Singapore*
[3]*Department of Electrical and Computer Engineering, National University of Singapore, Singapore 117576, Singapore and Data Storage Institute, 5 Engineering Drive 1, Singapore 117608, Singapore*

(Received 5 November 2008; accepted 13 December 2008; published online 8 January 2009)

In this letter, using both off-resonant and resonant Raman spectroscopic techniques, the correlation of optical phonons and structural disorder in $As^+$ implanted ZnO single crystals has been investigated. An additional broad peak shoulder at 550 $cm^{-1}$ between the transverse optical and longitudinal optical (LO) phonons was clarified to be resonant Fröhlich optical phonon mode in the framework of effective dielectric function. Under resonance condition, an asymmetric broadening and softening of the LO phonon along with a blueshifted luminescent peak revealed the decreasing phonon coherent length and nanocrystallization with increasing fluence, respectively, in good agreement with the observations of transmission electron microscopy and atomic force microscopy. © *2009 American Institute of Physics*. [DOI: 10.1063/1.3067997]

Recently, ion implantation technique has been attempted in ZnO to realize *p*-type conductivity.[1–3] However, the ion-beam interaction introduces lattice disorder and extended defect regardless of the pronounced dynamic annealing process.[4–8] Hence, a thorough understanding of damage accumulation and stability of implantation induced defects is highly desirable. Raman scattering, as a nondestructive method, could be employed to monitor the implantation induced lattice modifications and disorders.[8–11] In ZnO, the anomalous vibrational band between 520 and 600 $cm^{-1}$ has been ascribed to the ion bombardment induced disorder-activated longitudinal optical (LO) modes,[8,10,11] while the similar bands, named as "surface optical phonons," also appeared in some ZnO nanostructures.[12,13] Recently, Friedrich and Nickel[9] clearly established that the 577 $cm^{-1}$ mode in the resonant Raman spectra of H- and N-implanted ZnO is due to the resonantly enhanced LO phonons via Fröhlich interaction. In fact, the frequencies of the Fröhlich modes can be tuned within the frequency gap between bulk transverse optical (TO) and LO phonons, strongly dependent on the environment of the host material lattice. In this letter, we revisit the interpretation of this anomalous vibrational band to be Fröhlich character in the framework of the effective dielectric function. The correlation of optical phonons with lattice disorder and surface modification has also been discussed.

The samples used were high quality single crystal ZnO (0001) grown by hydrothermal method. 150 keV $As^+$ ions were homogeneously implanted at the fluence range from $2\times10^{13}$ to $5\times10^{15}$ $cm^{-2}$ at room temperature, and the samples were tilted 7° relative to the incident beam to minimize channeling effect. Figure 1(a) shows the bright-field cross-sectional transmission electron microscopy (XTEM) of ZnO implanted with $As^+$ fluence of $5\times10^{15}$ $cm^{-2}$. Three regions with distinct image contrast are observed, as denoted by A, B, and C and shown in Figs. 1(b)–1(d), respectively. Small defect clusters or dislocations are visible inside region C, as accompanied by numerous stacking faults perpendicular to the [0001] direction. The upper edge of the buried damage region B contains minimal damages as a consequence of dynamic annealing during implantation,[6,7] and the defects are larger in size and smaller in density, exhibiting asymmetric distribution along depth. The surface layer indicated by A comprises misoriented nanocrystallites.

The Raman measurements were carried out at room temperature using the $Ar^+$ laser (514 nm) and He–Cd laser

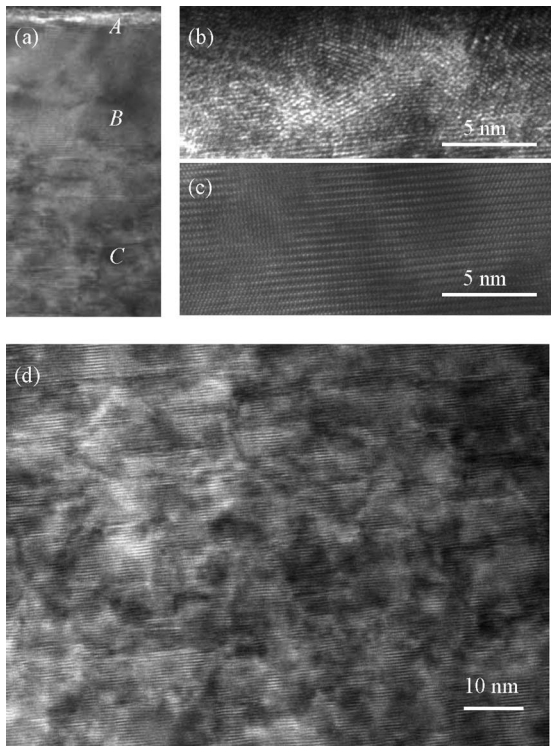


FIG. 1. (a) High-resolution bright-field XTEM image of $5\times10^{15}$ $cm^{-2}$ $As^+$ implanted ZnO single crystal, and (b)–(d) are the enlarged images of regions A–C denoted in image (a), respectively.

a)Author to whom correspondence should be addressed. Electronic mail: yejd@ime.a-star.edu.sg.

 

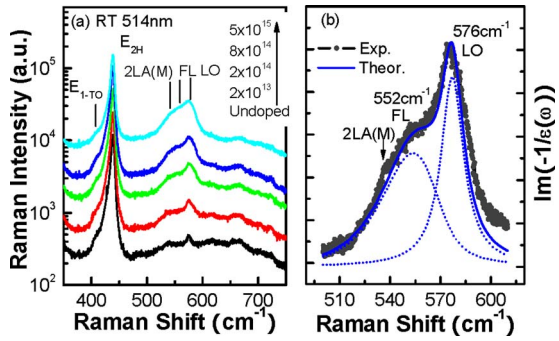


FIG. 2. (Color online) (a) Off-resonant Raman spectra of undoped and different fluence implanted ZnO. (b) The line shape fitting and experimental phonon peaks of $As^+$ implanted ZnO with a fluence of $8\times10^{14}$ $cm^{-2}$.

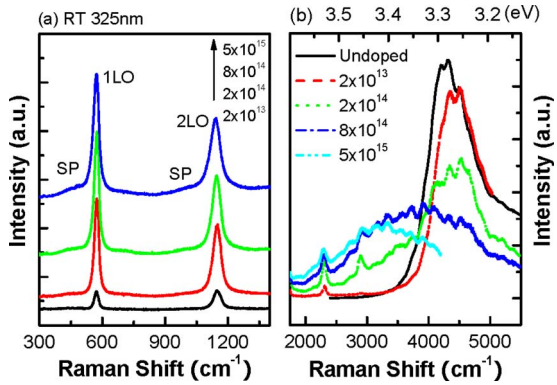


FIG. 3. (Color online) Resonance Raman spectra of As-implanted ZnO with different fluences in the ranges of (a) 350–750 $cm^{-1}$ and (b) 1800–5500 $cm^{-1}$.

(325 nm) as the excitation sources for off-resonant and resonant measurement, respectively. Figure 2(a) shows the off-resonant Raman spectra of ZnO samples implanted with different $As^+$ fluences. The $E_{2H}$ modes around 437 $cm^{-1}$ decreased in intensity and broadened gradually with the increasing fluence, while the intensity of forbidden LO modes around 575 $cm^{-1}$ increased gradually, as compared to that of undoped ZnO. These features revealed an increased lattice disorder within the implanted layer. The distinct broad modes around 520–580 $cm^{-1}$ become intense accompanied by LO modes, as commonly observed in the Raman spectra of implanted ZnO.[8–11] Numerous studies correlate this anomalous vibration mode to be the disorder-active LO phonons, originating from high density of phonon states of high-energy phonon branch.[8,10,11] However, the similar vibration bands have also been reported as the interfacial optical phonons, exhibiting strong dependence on the dielectric constant of the surrounding medium.[12–14] In fact, these two interpretations are consistent and the physics behind is resonant Fröhlich optical phonons.[15–19] The total vacancy concentration caused by ion bombardment is much higher than that of the implanted ion. Even if 1% of vacancies could be present, its density is still as high as $10^{21}$ $cm^{-3}$ for ion fluence of $5\times10^{15}$ $cm^{-2}$. In other words, the buried damage layer consists of high density vacancy clusters and the relative porosity of ~1% of implanted layer. For porous material, the effective dielectric function will be different with bulk material,

$$\varepsilon_{\parallel} = (1-c)\varepsilon^{\mathrm{vac}} + c\varepsilon_{\parallel}^{\mathrm{ZnO}}, \tag{1}$$

$$\varepsilon_{\perp} = \frac{(1+c)\varepsilon_{\perp}^{\mathrm{ZnO}} + (1-c)\varepsilon^{\mathrm{vac}}}{(1-c)\varepsilon_{\perp}^{\mathrm{ZnO}} + (1+c)\varepsilon^{\mathrm{vac}}}\varepsilon^{\mathrm{vac}}, \tag{2}$$

where $c$ is the relative porosity of implanted ZnO and $\varepsilon^{\mathrm{vac}}=1$. Taking into consideration the plasmon contribution, the dielectric functions of ZnO are written as

$$\varepsilon_{\parallel(\perp)}^{\mathrm{ZnO}} = \varepsilon_{A_1(E_1)} = \varepsilon_{\infty}\left[\frac{\omega_{A_{1L}(E_{1L})}^2 - \omega^2 - i\omega\gamma}{\omega_{A_{1T}(E_{1T})}^2 - \omega^2 - i\omega\gamma} - \frac{\omega_p^2}{\omega^2 + i\omega\Gamma}\right], \tag{3}$$

where $\omega_{A_1(E_1)}$ is the uncoupled phonon frequency of the $A_1$ $(E_1)$-type mode, $\omega_p = \sqrt{Ne^2/\varepsilon_{\infty}m^*}$ is the plasmon frequency, $\Gamma(=e/\mu m^*)$ is plasmon damping rate, $\gamma$ is phonon damping rate, and $N$ and $m^*$ represent free carrier density and effective mass of electron, respectively. Given that $\omega_{A_{1L}}$ $=574$ $cm^{-1}$, $\omega_{A_{1T}}=380$ $cm^{-1}$, $\omega_{E_{1T}}=408$ $cm^{-1}$, $\varepsilon_{\infty}=3.7$, $N=1.65\times10^{17}$ $cm^{-3}$, $m^*=0.28m_e$, and mobility $\mu=5$ $V\,s/cm^2$, the Fröhlich mode will be originated from the damaged layer $(c\to0)$ in terms of $\varepsilon_{\perp}^{\mathrm{ZnO}}+\varepsilon^{\mathrm{vac}}=0$, and the corresponding frequency is 553 $cm^{-1}$, which is in the region of the broad shoulder as shown in Fig. 2.

Next, we employ the same approach as described in the case of Raman spectra of porous GaP (Ref. 16) and GaN nanocolumn[15] to probe the Raman peak appearing at 550 $cm^{-1}$. This peak was deconvoluted by multi-Lorentzian fitting, where the Raman line shape is derived by the dominant excitation of extraordinary phonons with the averaging weight due to multiple scattering,[15,16]

$$I_{\mathrm{eo}} \sim \mathrm{Im}[-1/(\varepsilon_{\parallel}\cos^2\theta + \varepsilon_{\perp}\sin^2\theta)]\exp(-\theta^2/\sigma^2), \tag{4}$$

where $\theta$ is the angle between the exciting light wave vector and the direction parallel to the $c$-axis. The best fit obtained in this way is shown in Fig. 2(b) by the dashed curve, which is in reasonable agreement with the experimental spectrum with porosity $c$ of 2.5%. We note that the broad shoulder below bulk LO mode is essentially due to the changes in the dielectric constant of buried damage region and thus can be employed to monitor the radiation effect on lattice modification. With increasing ion fluence, much increased in intensity. However, no measurable shift in this mode can be observed under off-resonant condition. This may be due to the competition of the decreasing effective dielectric constant and increasing plasmon frequencies caused by vacancies-induced porosity and high free carrier concentration in the buried damage layer, respectively.[16,17]

The implantation induced structural modification at the surface has been further addressed by the resonant Raman spectrum with a small penetration depth of 325 nm line laser. The resonant Raman spectra in Fig. 3(a) show that the intensity of LO phonons is enhanced greatly under resonance condition, which implies the strong contribution of Fröhlich interaction to the forbidden LO phonon scattering efficiency.[20] Another characteristic feature is that the asymmetric broadening and measurable shift in the LO and two LO phonons $\Delta\omega$ in the range between 3.5 and 8.7 $cm^{-1}$ as the fluence increases from $2\times10^{13}$ to $5\times10^{15}$ $cm^{-2}$, respectively. Ion implantation is an effective method to modify the surface porosity and nanocrystallization.[7,21,22] It is evidently observed by atomic force microscopy (AFM) in Figs. 4(b) and 4(c) that many nanosized voids are exposed to the surface, resulting in the surface roughening. The root-mean-square

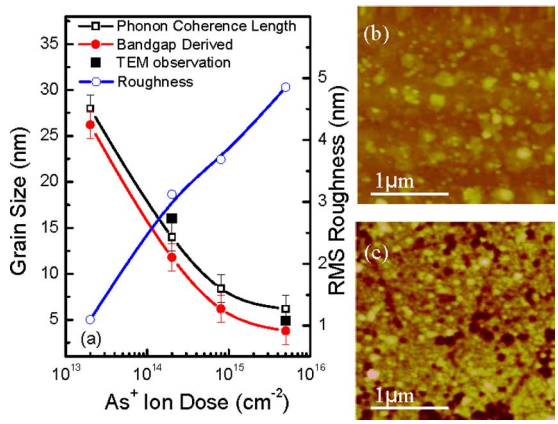


FIG. 4. (Color online) (a) The calculated grain sizes and coherence length as a function of $As^+$ ion fluences. The coherence length was estimated from the frequency shift of LO phonons in terms of well-known Phonon Confinement Model. The grain sizes were estimated from the relationship between band gap and size of nanocrystallites in terms of effective mass model. (b) and (c) are the AFM images of samples implanted with $As^+$ fluences of $2\times10^{14}$ and $5\times10^{15}$ $cm^{-2}$, respectively.

roughness increased from 1.09 to 4.86 nm with increasing ion fluence from $2\times10^{13}$ to $5\times10^{15}$ $cm^{-2}$. The lattice within surface layer A extended only several nanometers and misoriented with each other. Thus, these misoriented nanocrystallites will enhance the strength of intrinsic Fröhlich interaction due to relaxation of the $q=0$ selection rules and $\sim q^2$ proportional dependence in the finite-size domain.[20] The related phonon coherence length ($L$) or the average size of the undamaged crystalline regions could be evaluated by the Raman shift of LO phonons in terms of the well-known phonon confinement spatial model.[23] The estimated phonon coherence lengths ($L$) shown in Fig. 4(a) decrease from 6.1 to 8 nm with ion fluencies increasing from $2\times10^{13}$ to $5\times10^{15}$ $cm^{-2}$, indicative of nanocrystallization processes during ion implantation.

The nanocrystallization effect of ion implantation is also reflected by the modification of band gap with implanted layer. Figure 3(b) shows the wide range resonance Raman spectra of samples with different ion fluences. Besides LO phonon peaks and interference oscillations, the broad peak of hot luminescence shows a distinct blueshift from 3.264 to 3.412 eV with increasing ion fluence of $2\times10^{13}$–$5\times10^{15}$ $cm^{-2}$. The electron energy loss spectra also exhibit a wide band gap of about 3.45 eV within the implanted layer for ion fluence of $5\times10^{15}$ $cm^{-2}$. The dominant origin of band gap widening should be the quantum confinement within the finite size of nanocrystallite, which has been extensively evaluated in other ZnO quantum structures.[24] Based on the effective mass model, the evaluated sizes of nanocrystallites increase from 3.8 to 26.2 nm with ion fluence increasing from $2\times10^{13}$ to $5\times10^{15}$ $cm^{-2}$, in reasonable agreement with the phonon coherence length estimated from LO phonon frequency shift, as shown in Fig. 4(a). The slight overestimate of phonon coherence length is due to the small redshift of LO phonons, which can be affected by other factors. First, the extrinsic Fröhlich interaction mediated by the localized electronic states bound to defect or impurity could enhance the forbidden scattering efficiency independent of wave vector $q$, and thus will not cause the shift in resonant LO phonons.[25] Second, the increase in free carrier concentration with increasing ion fluence will cause the increased frequencies of LO-plasmon coupling modes. This will in turn lead the blueshift of LO phonons. The estimated values of LO phonon and band gap were very close to the statistic size by TEM investigation in Fig. 1(a). This indicates the validity and feasibility of nondestructive analysis on damages and disorders in implanted sample by Raman measurement.

In summary, we have investigated the correlation of Fröhlich optical phonons with lattice disorder and surface modification in As-implanted ZnO. The asymmetric broadening and softening of Fröhlich optical phonons revealed the decreased phonon coherence length in the implanted layer, indicative of nanocrystallines and nanoporosity. The band gap widening by implantation also confirmed the nanocrystallization process, in good agreement with the observations of TEM and AFM.

This work was supported by the Singapore Agency for Science, Technology and Research (A*STAR), under SERC Grant No. 0521260095.

[1]Q. L. Gu, C. C. Ling, G. Brauer, W. Anwand, W. Skorupa, Y. F. Hsu, A. B. Djurisic, C. Y. Zhu, S. Fung, and L. W. Lu, Appl. Phys. Lett. **92**, 222109 (2008).
[2]G. Braunstein, A. Muraviev, H. Saxena, N. Dhere, V. Richter, and R. Kalish, Appl. Phys. Lett. **87**, 192103 (2005).
[3]T. S. Jeong, M. S. Han, C. J. Youn, and Y. S. Park, J. Appl. Phys. **96**, 175 (2004).
[4]H. von Wenckstern, R. Pickenhain, H. Schmidt, M. Brandt, G. Biehne, M. Lorenz, M. Grundmann, and G. Brauer, Appl. Phys. Lett. **89**, 092122 (2006).
[5]U. Wahl, E. Rita, J. G. Correia, A. C. Marques, E. Alves, and J. C. Soares, Phys. Rev. Lett. **95**, 215503 (2005).
[6]S. O. Kucheyev, J. S. Williams, C. Jagadish, J. Zou, C. Evans, A. J. Nelson, and A. V. Hamza, Phys. Rev. B **67**, 094115 (2003).
[7]V. A. Coleman, H. H. Tan, C. Jagadish, S. O. Kucheyev, and J. Zou, Appl. Phys. Lett. **87**, 231912 (2005).
[8]L. Artus, R. Cusco, E. Alarcon-Llado, G. Gonzalez-Diaz, I. Martil, J. Jimenez, B. Wang, and M. Callahan, Appl. Phys. Lett. **90**, 181911 (2007).
[9]F. Friedrich and N. H. Nickel, Appl. Phys. Lett. **91**, 111903 (2007).
[10]J. B. Wang, H. M. Zhong, Z. F. Li, and W. Lu, Appl. Phys. Lett. **88**, 101913 (2006).
[11]M. Schumm, M. Koerdel, S. Muller, H. Zutz, C. Ronning, J. Stehr, D. M. Hofmann, and J. Geurts, New J. Phys. **10**, 043004 (2008).
[12]H. Zeng, W. Cai, B. Cao, J. Hu, Y. Li, and P. Liu, Appl. Phys. Lett. **88**, 181905 (2006).
[13]P. M. Chassaing, F. Femangeot, V. Paillard, A. Zwick, N. Combe, C. Pages, M. L. Kahn, A. Maisonnat, and B. Chaudret, Phys. Rev. B **77**, 153306 (2008).
[14]V. A. Fonoberov and A. A. Balandin, Phys. Rev. B **70**, 233205 (2004).
[15]I. M. Tiginyanu, A. Sarua, G. Irmer, J. Monecke, S. M. Hubbard, D. Pavlidis, and V. Valiaev, Phys. Rev. B **64**, 233317 (2001).
[16]A. Sarua, J. Monecke, G. Irmer, I. M. Tiginyanu, G. Gartner, and H. L. Hartnagel, J. Phys.: Condens. Matter **13**, 6687 (2001).
[17]G. Irmer, J. Raman Spectrosc. **38**, 634 (2007).
[18]R. Gupta, Q. Xiong, G. D. Mahan, and P. C. Eklund, Nano Lett. **3**, 1745 (2003).
[19]Q. Xiong, J. G. Wang, O. Reese, L. C. Lew, and P. C. Eklund, Nano Lett. **4**, 1991 (2004).
[20]R. M. Martin and T. C. Damen, Phys. Rev. Lett. **26**, 86 (1971).
[21]F. Gloux, T. Wojtowicz, P. Ruterana, K. Lorenz, and E. Alves, J. Appl. Phys. **100**, 073520 (2006).
[22]M. Ishimaru, Y. Hirotsu, F. Li, and K. E. Dickafus, Appl. Phys. Lett. **77**, 4151 (2000).
[23]K. F. Lin, H. Cheng, H. Hsu, and W. Hsieh, Appl. Phys. Lett. **88**, 263117 (2006).
[24]K. F. Lin, H. Cheng, H. Hsu, L. Lin, and W. Hsieh, Chem. Phys. Lett. **409**, 208 (2005).
[25]J. Menendez and M. Cardona, Phys. Rev. B **31**, 3696 (1985).